JGR Planets

RESEARCH ARTICLE
10.1029/2022JE007398

Partially-Saturated Brines Within Basal Ice or Sediments Can Explain the Bright Basal Reflections in the South Polar Layered Deposits

D. E. Stillman[1], E. Pettinelli[2], S. E. Lauro[2], E. Mattei[2], G. Caprarelli[3], B. Cosciotti[2], K. M. Primm[4], and R. Orosei[5]

[1]Department of Space Studies, Southwest Research Institute, Boulder, CO, USA, [2]Mathematics and Physics Department, Roma Tre University, Rome, Italy, [3]Centre for Astrophysics, Institute for Advanced Engineering and Space Sciences, University of Southern Queensland, Toowomba, QLD, Australia, [4]Planetary Science Institute, Tucson, AZ, USA, [5]Istituto di Radioastronomia (IRA), Istituto Nazionale di Astrofisica (INAF), Bologna, Italy

Key Points:

- Brines possess a significantly higher real part of dielectric permittivity and Direct Current (DC) conductivity than dry and frozen minerals
- Salt enhancements of 5–16 times the salt-regolith concentration at the Phoenix landing site is needed in brine-sediment mixtures
- The basal unit must be equal or greater than the eutectic temperature of calcium perchlorate (197.3 ± 0.2 K) to allow for brine formation

Supporting Information:

Supporting Information may be found in the online version of this article.

Correspondence to:

D. E. Stillman,
dstillman@boulder.swri.edu

Citation:

Stillman, D. E., Pettinelli, E., Lauro, S. E., Mattei, E., Caprarelli, G., Cosciotti, B., et al. (2022). Partially-saturated brines within basal ice or sediments can explain the bright basal reflections in the south polar layered deposits. *Journal of Geophysical Research: Planets*, *127*, e2022JE007398. https://doi.org/10.1029/2022JE007398

Received 31 MAY 2022
Accepted 28 SEP 2022

Author Contributions:

Conceptualization: D. E. Stillman, E. Pettinelli, S. E. Lauro, E. Mattei, G. Caprarelli, B. Cosciotti, R. Orosei
Formal analysis: D. E. Stillman
Funding acquisition: D. E. Stillman
Investigation: D. E. Stillman, K. M. Primm
Methodology: D. E. Stillman, K. M. Primm
Project Administration: D. E. Stillman, E. Pettinelli
Supervision: E. Pettinelli

Abstract Strong radar reflections have been previously mapped at the base of the Martian South Polar Layered Deposits. Here, we analyze laboratory measurements of dry and briny samples to determine the cause of this radar return. We find that liquid vein networks consisting of brines at the grain boundaries of ice crystals can greatly enhance the electrical conductivity, thereby causing strong radar reflections. A brine concentration of 2.7–6.0 vol% in ice is sufficient to match the electrical properties of the basal reflection as observed by Mars Advanced Radar for Subsurface and Ionospheric Sounding (MARSIS). When brine is mixed with sediments, the brine-ice mixture in the pores must be 2–5 times more concentrated in salt, increasing the brine concentration to 6.3–29 vol%. Our best fit of the median observed MARSIS value suggests a salt-bulk sample concentration of ∼6 wt%. Thus, salt enhancement mechanisms on the order of a magnitude greater than the Phoenix landing site are needed. To form brine, the basal reflector must reach a temperature greater than the eutectic temperature of calcium perchlorate of 197.3 ± 0.2 K, which may be possible if more complex thermal modeling is assumed. Colder metastable brines are possible, but stability over millions of years remains unclear. Conversely, gray hematite with a concentration of 33.2–59.0 vol% possess electrical properties that could cause the observed radar returns, but require concentrations 2–3 times larger than anywhere currently detected. We also argue that brines mixed with high-surface-area sediments, or dry red hematite, jarosite, and ilmenite cannot create the observed radar returns at low temperatures.

Plain Language Summary Previous research has detected strong radar reflections from the interface between Mars' southern ice cap and their underlying sediments over a region with an area of 20 × 30 km and 1.5 kms beneath the surface. Radar reflections are caused by changes in electrical properties. Here, we analyze electrical property laboratory measurements of materials under Mars-like conditions. We find that a small amount of brine in ice samples could create strong radar reflections similar to those that are observed. A greater concentration of salt is needed in sediment-ice mixtures. We suspect that the sublimation of a previous version of the ice cap may have deposited salt via sublimation in the base of the current ice cap. Additionally, the temperature at the base of the ice cap must be warmer than simple thermal models estimate, we suggest insulating materials such as CO_2 ice may be incorporated into the ice cap. Additionally, dry gray hematite could also cause the observed radar returns, but must be even more concentrated than anywhere yet discovered on Mars. We can also rule out any brines mixed with clays, or dry red hematite, jarosite, and ilmenite as they cannot create the observed radar returns at low temperature.

1. Introduction

The Mars Advanced Radar for Subsurface and Ionospheric Sounding (MARSIS) instrument on Mars Express has detected strong subsurface radar reflections in the region of Ultimi Scopuli (81°S, 193°E), within the South Polar Layered Deposits (SPLD) (Lauro et al., 2021; Orosei et al., 2018). These subsurface reflections are ∼10 dB greater in power than the surrounding reflections and ∼3 dB greater than the reflections from the surface (Orosei et al., 2018). The reflectors are located at the base of the SPLD, approximately 1.5 km below the topographic surface. Because data acquired by MARSIS do not separate the real (ε') and imaginary (ε'') parts of the complex permittivity of reflectors, the apparent permittivity (ε_a), a single parameter accounting for both ε' and ε'' (Mattei

Writing – original draft: D. E. Stillman
Writing – review & editing: E. Pettinelli, S. E. Lauro, E. Mattei, G. Caprarelli, B. Cosciotti, K. M. Primm

et al., 2022; ref. to §2.2) is commonly reported. In their investigation of the SPLD, Orosei et al. (2018) obtained reflectivities characterized by a median ε_a value of 33 ± 1 at 4 MHz. Using a threshold value of $\varepsilon_a = 15$, the largest reflective zone is ~20 × 30 km (Lauro et al., 2021). Furthermore, Lauro et al. (2021) also detected at least three other smaller locations, about 10 km across, within 120 km of the largest anomaly.

The high reflectivity values observed by MARSIS (Orosei et al., 2018) were found to have a first and third quartile values ε_a of 16 and 91, respectively. Such high values of ε_a limit the number of materials that could cause such reflections. Three categories of materials have thus far been proposed to explain the high reflectivity values: clays with adsorbed water (Smith et al., 2021); dry minerals and rocks with high iron content (Bierson et al., 2021; Grima et al., 2022); and saline ice (Bierson et al., 2021).

Smith et al. (2021) suggested that the dielectric relaxation of clay with adsorbed water at the base of the SPLD could result in high ε_a values at the presumed basal temperature in Ultimi Scopuli. However, Smith et al.'s (2021) data were measured at 230 K and are inconsistent with similar types of measurements as reported in the literature (Cunje et al., 2018; Kułacz & Orzechowski, 2019; Lorek & Wagner, 2013; Mattei et al., 2022; Moore & Maeno, 1993; Stillman & Grimm, 2011a; Stillman et al., 2010).

Bierson et al. (2021) suggested that jarosite and red hematite are a possible source for the bright reflection. However, the literature does not support this hypothesis as dry jarosite and red hematite have a low ε' (Robinson & Friedman, 2003; Stillman & Olhoeft, 2008). Robinson and Friedman (2003) measured that a soil sample of red hematite with 50.5% porosity with a bulk $\varepsilon' = 4.5$, which is consistent with measurements reported by Stillman and Olhoeft (2008). Bierson et al. (2021) used the estimate of the grain or solid permittivity of $\varepsilon' = 18.1$ for red hematite (Robinson & Friedman, 2003). Assuming minimal porosity of 10% for a hematite-rich rock, using Robinson and Friedman (2003) mixing models, we estimate a bulk ε' value of 10.8, which is lower than the observed first quartile value.

Bierson et al. (2021) suggested that the conductivity of saline ice, that is, ice with a bulk salt mass concentration range of 0.1–3.5 wt%, could return ε_a values within range of those observed at Ultimi Scopuli. Liquid brines have high ε' (~80) and are highly conductive; thus, brines in ice or sediments can plausibly create ε_a values within range of those observed by MARSIS (Mattei et al., 2022). Grima et al. (2022) suggested that measurements of bulk $\varepsilon' > 16$ have been reported for ilmenite ($FeTiO_3$) and basalts (Parkhomenko, 1967; Rust et al., 1999; Shmulevich et al., 1971).

For this research, we use the first quartile, median, and third quartile values of the 4-MHz MARSIS permittivity contrast at the base of the SPLD (Orosei et al., 2018). We then use our laboratory measurements of electrical properties of salt mixtures with and without sediments to determine the concentrations of salt that match the MARSIS observed values at SPLD-like temperatures. We also address the dry material interpretation through our laboratory experiments on ilmenite, and further discuss dielectric permittivity of basalt and gray hematite based on measurements in the literature.

2. Background

2.1. MARSIS

MARSIS acquires data on four channels, with center frequencies of 1.8, 3, 4, and 5 MHz, each with a bandwidth of 1 MHz (e.g., Picardi et al., 2005). The MARSIS data set used by Orosei et al. (2018) and Lauro et al. (2021) was acquired in raw-data mode, where raw amplitudes are sent to the ground without onboard synthetic-aperture radar processing. This ensures the amplitudes were as accurate as possible (Lauro et al., 2021), and enhances the horizontal resolution as groups of 100–300 raw echo gathers are not averaged together by the onboard processing. The 4 MHz center frequency data is the most complete set of MARSIS observations around the Ultimi Scopuli region (Lauro et al., 2021). The radius of the first Fresnel zone is ~3.5–6 km depending on satellite altitude (300–800 km; Orosei et al., 2018), while the more conservative pulse limited criterion, has a diameter of 7.5 km assuming a satellite altitude of 400 km (Lauro et al., 2021). Thus, the anomalous areas are larger than the pulse limited criterion. Lastly, the vertical resolution is ~55 m, after range compression and Hanning windowing when assuming an $\varepsilon' = 3.1$ of pure ice (Lauro et al., 2021).

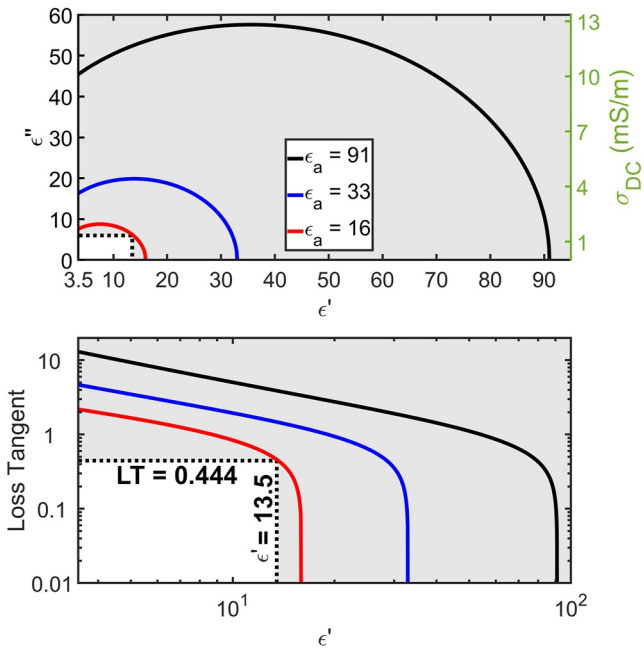

Figure 1. The solid lines display possible (a) ε' and ε'' and (b) ε' and loss tangent ($\varepsilon''/\varepsilon'$) that will combine for an ε_a equal to the first, second (median), and third quartile observed values of 16, 33, and 91, respectively. If a laboratory sample has a measured ε' and ε'' value of <13.5 and < 6 (loss tangent of 0.444) at 4 MHz, respectively, then ε_a cannot obtain the first quartile Mars Advanced Radar for Subsurface and Ionospheric Sounding (MARSIS) observed ε_a value. Note we assumed an ε' and ε'' of 3.5 and 0 for the South Polar Layered Deposits (SPLD). Additionally, the right *y*-axis in (a) shows the necessary values of σ_{DC}, if we assume all losses are conductive. Thus, σ_{DC} must be >1.3 mS m^{-1} to obtain the first quartile MARSIS observed ε_a value.

2.2. Electrical Properties

The electrical properties of the material control the speed at which radar waves propagate, the amount of energy that is attenuated, and how much energy is reflected at discontinuities. Here and in the following discussion, we ignore the effects of the magnetic permeability, given its small variability (Stillman & Olhoeft, 2008). The real part of the relative dielectric permittivity ε' primarily controls the speed at which radar waves propagate through the material. In most dry rocks at radar frequencies, ε' can be estimated using the following equation:

$$\varepsilon' = (1.93 \pm 0.17)^{\rho}, \tag{1}$$

where ρ is the bulk density of the rock or soil in g cm^{-3} (Olhoeft & Strangway, 1975). The imaginary part of the relative dielectric permittivity ε'' primarily controls the attenuation of radar waves through the material, and is a summation of losses due to dielectric relaxations ε''_p and Direct Current (DC) electrical conductivity σ_{DC},

$$\varepsilon'' = \varepsilon''_p + \frac{\sigma_{DC}}{2\pi f \varepsilon_o}, \tag{2}$$

where f is the frequency of the radar energy and ε_o is the dielectric permittivity in vacuum (8.854×10^{-12} F m^{-1}).

Next, we convert ε' and ε'' into ε_a (Mattei et al., 2022) using

$$\varepsilon_a = \varepsilon_1 \frac{\varepsilon_1 + |\varepsilon_2| + \sqrt{\varepsilon_1^2 + |\varepsilon_2|^2 - 2\varepsilon_1\varepsilon'_2}}{\varepsilon_1 + |\varepsilon_2| - \sqrt{\varepsilon_1^2 + |\varepsilon_2|^2 - 2\varepsilon_1\varepsilon'_2}}, \tag{3}$$

where ε_1 is the ε' of the SPLD assumed to be 3.5, ε'' of the SPLD is assumed to be zero, and magnitude of the permittivity of the basal reflector is

$$|\varepsilon_2| = \sqrt{\varepsilon'^2_2 + \varepsilon''^2_2}. \tag{4}$$

An evaluation of Equation 3 shows that if the measured values of ε'_2 and ε''_2 are below 13.5 and 6, then ε_a cannot obtain the MARSIS observed first quartile value (Figure 1).

Electrical properties are frequency dependent because different polarization mechanisms separate charges at different speeds (e.g., Stillman et al., 2010; Stillman & Olhoeft, 2008). To model the material's frequency dependence, we use the Cole-Cole equation (Cole & Cole, 1941; Stillman & Olhoeft, 2008). The time it takes for a bound charge to separate is also temperature dependent, and is modeled with a Boltzmann temperature dependence (e.g., Stillman & Olhoeft, 2008, and refs. therein). Thus, frequency-dependent materials are also temperature dependent. The Cole-Cole and Boltzmann models allow us to extrapolate and interpolate electrical properties in frequency and temperature. Thus, ε' and ε'' measured to 1 MHz can be extrapolated to comprise the MARSIS frequency range of 2–5 MHz (e.g., Stillman & Grimm, 2011b). Additionally, as the frequency dependence shifts to lower frequency at colder temperatures, we can test whether the extrapolation is valid (Stillman & Grimm, 2011b).

2.3. Formation of Brines

Salt-H_2O mixtures are characterized by four distinct phases (Figure 2a):

1. Brine: when the temperature of the mixture is above the melting temperature;
2. Brine + ice: when the temperature of a sub-eutectic concentration (<49.8 wt% for $Ca(ClO_4)_2$) is below the melting temperature, but above the eutectic temperature;

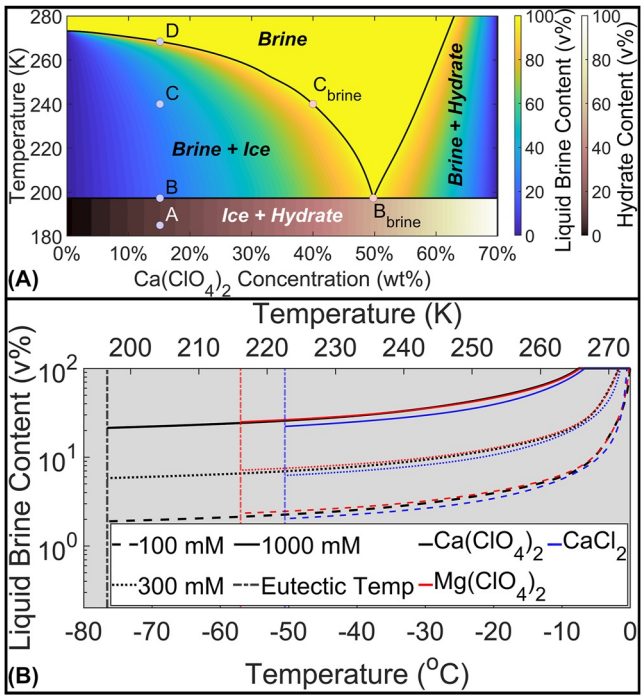

Figure 2. (a) Phase diagram of $Ca(ClO_4)_2$ with colored contours of bulk brine (parula colormap) and hydrate (pink colormap) concentrations. For example, a 700 mM (15.1 wt%) $Ca(ClO_4)_2$ sample at 185 K (Point A) has a hydrate content of ∼12 vol%. At the eutectic temperature, the hydrate and ice melts to form a brine with a eutectic concentration (Point B_{brine}) and with a liquid content of ∼14 vol%. At 240 K, the amount of liquid brine in the salt-H_2O mixture is ∼22% (Point C), while the brine concentration is 40 wt% (Point C_{brine}). The sample then completely melts at 268.4 K (Point D). (b) Volume percent of brine at 100, 300, and 1,000 mM versus temperature. The eutectic temperatures for $Ca(ClO_4)_2$, $Mg(ClO_4)_2$, and $CaCl_2$ are ∼197.3, 216, 223 K, respectively.

3. Brine + hydrate: when the temperature of a super-eutectic concentration is below the melting temperature, but above the eutectic temperature; and
4. Ice + hydrate: when the temperature of a mixture is below the eutectic temperature.

Here we focus on the brine + ice phase for sub-eutectic concentrations. As a sub-eutectic concentration (<49.8 wt% for $Ca(ClO_4)_2$) sample begins to freeze below the melting point, H_2O is fractionated out of the system as pure ice (or nearly pure ice if Cl^-, F^-, or NH_4^+; for more see Gross et al., 1977; Petrenko & Whitworth, 1999; Stillman et al., 2013b; Stillman et al., 2013a) and the salt-H_2O mass concentration increases in the liquid brine until it reaches the eutectic concentration at the eutectic temperature. The amount of liquid brine present at the eutectic depends on its initial concentration and salt type (Figure 2). The melt accumulates at the boundaries of the ice grains. Even low salinity brines (e.g., ∼3 mM, ∼0.03 mass%, or ∼0.06 vol%; Grimm et al., 2008) are electrically conductive, forming electrically connected networks across the ice matrix, termed Liquid Vein Networks (LVNs). Thus, salt-H_2O mixtures display high σ_{DC} even when most of the ice is frozen (Grimm et al., 2008; Stillman et al., 2010). When temperatures drop below the eutectic temperature, the entire system freezes into ice and hydrate, and σ_{DC} drops significantly.

2.4. Estimated Basal SPLD Temperature

Estimates of the values of SPLD basal temperatures in Ultimi Scopuli have been recently published (Egea-González et al., 2022; Ojha et al., 2021; Sori & Bramson, 2019), and are heavily dependent upon the heat flow from the planetary interior, and the thermal conductivity of the SPLD, both of which are not fully constrained. Assuming a temperature-dependent thermal conductivity of pure H_2O ice for the SPLD, a heat flow >84 mW/m^2 is required to allow liquid Ca-perchlorate brine to form. For a more realistic heat flow range of 14–25 mW m^{-2} (Parro et al., 2017), a basal temperature of ∼171–176 K is obtained (Sori & Bramson, 2019). Egea-González et al. (2022) found a basal temperature range of 175–187 K using the maximum surface heat flow (32 mW m^{-2}) by assuming a dust proportion of 15%. However, recent Insight seismic data suggests an enhancement of radioactive elements in the Martian upper crust suggesting that surface heat flow may need to be revised upward (Khan et al., 2021). Additionally, inclusion of CO_2 ice into H_2O ice layers or as pure CO_2 layers within the SPLD could further enhance basal temperatures (Wieczorek, 2008), as CO_2 ice has a thermal conductivity that is 5–6 times lower than that of H_2O ice (e.g., Mellon, 1996).

3. Methods

Low-frequency measurements were conducted at Southwest Research Institute in Boulder Colorado. Solutions of salt-H_2O mixtures were freshly prepared before each measurement. For measurements of salt-H_2O mixtures, the liquid solution was poured into the three-electrode sample holder with a Teflon cup (Solartron 12962 and 12964A). For measurements of salt-H_2O mixtures with Martian analogs, the analogs (e.g., clays, sands, ilmenite) were dried in a vacuum at ∼1 mbar and ∼383 K until their mass changed by less than 0.5% over a ∼12-hr period. The granular analog material was then spooned into the Teflon cup sample holder with a spatula, then the liquid solution was poured into the granular material. Lastly, the sample was mixed with a spatula to ensure homogeneity. The material thus homogenized was placed in a holder 3.5 cm in diameter and ∼0.6 cm thick, and holder was then placed into the sample chamber.

The sample chamber has been previously described (Grimm et al., 2008; Stillman et al., 2010). For measurements made after Sept 2019, we used a custom vacuum chamber placed in the Ultra-Low freezer (So-Low C85-9). Dry

materials were measured in vacuum of ~1 mbar, whereas samples containing ice were measured at atmospheric pressure.

The sample holder sits on a liquid nitrogen cold plate so that temperatures below 180 K can be obtained. Silicon diode (Lake Shore Cryotronics DT-670) temperature sensors are used to measure the sample temperature on the Teflon cup and a second sensor controls two 25 W cartridge heaters (Lake Shore Cryotornics HTR-25-100) via a temperature controller (Lake Shore Cryotronics 331). The sample is connected via Boynet Neill-Concelman cables to a Solartron 1260A impedance analyzer and a Solartron 1296A dielectric interface. The sample temperature is then lowered to reach a temperature 2 K below its freezing point for 1 hr to initialize crystallization. The temperature is subsequently decreased to 10 K below the freezing point for 2 hr, to ensure crystallization of any metastable water. Reheating of the sample is carried out by raising the temperature back to 2 K below the freezing point for 3 hr. This process guarantees formation of stable LVNs for the entire duration of the experiment, reducing the rate of cracking in the sample, and avoiding the effect of rapid recrystallization. The temperature of the sample is then lowered at a rate of $\leq$1 K min^{-1} to the desired temperature. The temperature is typically lowered to 10–20 K below the eutectic temperature, in an attempt to ensure that any metastable brine is frozen before starting the warming cycle measurements. Electrical property measurements are conducted non-stop as soon as the sample's σ_{DC} drops below 0.1 S/m, which is the upper detection limit of σ_{DC}. After obtaining the lowest temperature value the sample is slowly heated. To increase temperature accuracy, the target temperature is held to within 0.2 K for at least 20 min. Typically, measurements are made over the range of 1–10^6 Hz, which takes ~6 min to acquire. However, as σ_{DC} increases, the lower frequency limit is also increased, which reduces the time required to measure a spectrum. Furthermore, once the sample reaches the frequency at which σ_{DC} dominates the electrical properties the uncertainly of ε' increases greatly.

Complex impedance, which is a function of frequency, is measured, and is then converted into the complex dielectric permittivity using the electrode geometry. Cole-Cole parameters of each spectrum were modeled by nonlinear curve fitting (Grimm et al., 2008; Stillman & Olhoeft, 2008; Stillman et al., 2013a, 2013b). The Cole-Cole parameters were then used to find ε_a at 4 MHz as a function of temperature.

4. Results and Interpretations

4.1. Dry Ilmenite

Dry granular ilmenite (purchased from Ward's Scientific) with 35.5% porosity and a bulk density of 3.07 g cm^{-3} possesses a significant σ_{DC} and a polarization mechanism that increases ε' and ε'' at MARSIS frequencies (Figure 3). The observed relaxation mechanism is known as an anomalous low-frequency dispersion (e.g., Jonscher, 1978, 1999; Shahidi et al., 1975; Stillman et al., 2010). Previously reported data indicate that ilmenite reaches a value of $\varepsilon' > 33$ at room temperature (Parkhomenko, 1967). In our experiments, at ~273 K, the ε_a of ilmenite does not approach the observed median, dropping below the observed first quartile value at temperatures <252.8 K. Therefore, we conclude that ilmenite is not a plausible candidate as the cause of the strong basal reflections at Ultimi Scopuli.

4.2. Chloride Salt-H_2O Mixtures

Chloride brines in ice were previously shown to obtain high values of σ_{DC} and ε'' at temperatures above their eutectic temperatures (Grimm et al., 2008). However, NaCl (Grimm et al., 2008) and $MgCl_2$ (Primm et al., 2020) have eutectic temperatures of 251 and 240 K, respectively, which are too high for these salts to be considered in the context of the SPLD. $CaCl_2$ has a much lower eutectic temperature of 223 K (Stillman et al., 2010). The ε_a data versus temperature and concentration show that a 100 mM (1.1 wt%) of $CaCl_2$ at the eutectic temperature has an ε_a equivalent to the observed first quartile value (Figure 4). The ε_a of the 1,000 mM (10 wt%) of $CaCl_2$ is larger than the observed third quartile value (Figure 4), indicating a lower concentration is needed to match the third quartile value.

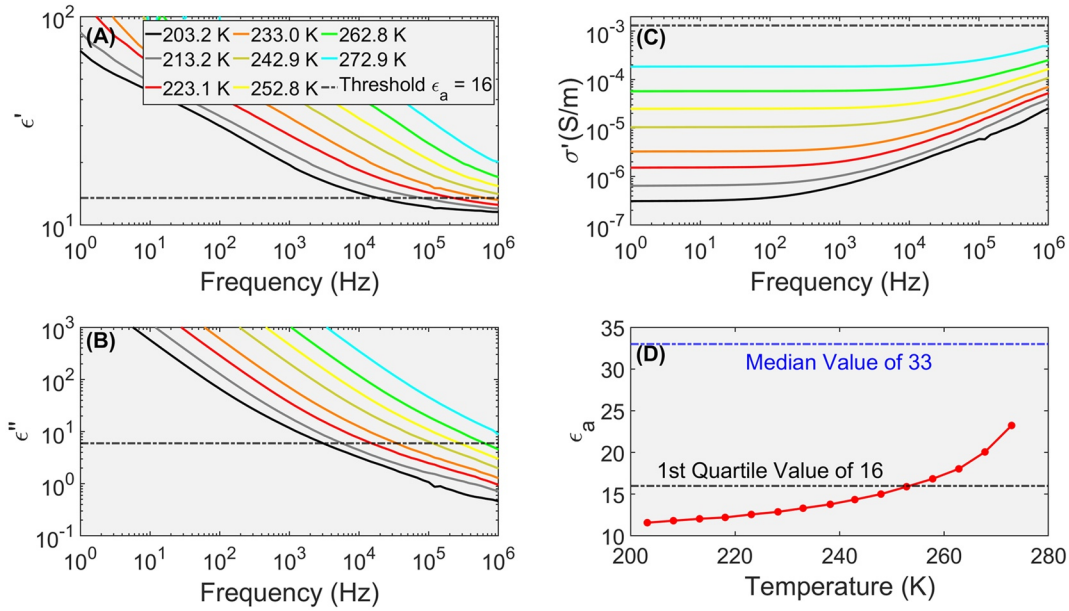

Figure 3. Real (a) and imaginary (b) part of the relative permittivity, real part of electrical conductivity (c) of ilmenite with 35.5% porosity. Ilmenite does have additional polarization mechanisms as well as σ_{DC} (shown by the plateau of σ' at low frequencies). The apparent permittivity (d) is calculated assuming an South Polar Layered Deposits (SPLD) with $\varepsilon' = 3.5$ as a function of temperature. This shows that the polarizations and σ_{DC} are not large enough to produce ε_a values within the observed range at temperatures below ~252.8 K.

4.3. Perchlorate Salt-H_2O Mixtures

4.3.1. Magnesium Perchlorate

With eutectic temperatures of 198 and 216 K (Toner et al., 2014) respectively, calcium and magnesium perchlorate brines have been proposed as the most plausible source for the bright basal reflections in Ultimi Scopuli (Lauro et al., 2021). Plots of ε_a versus temperature and concentration show that a concentration of 100 mM (2.2 wt%) of $Mg(ClO_4)_2$ is just below the observed first quartile value (Figure 5), while 500 mM (10 wt%) of $Mg(ClO_4)_2$ is greater than the observed third quartile value (Figure 5).

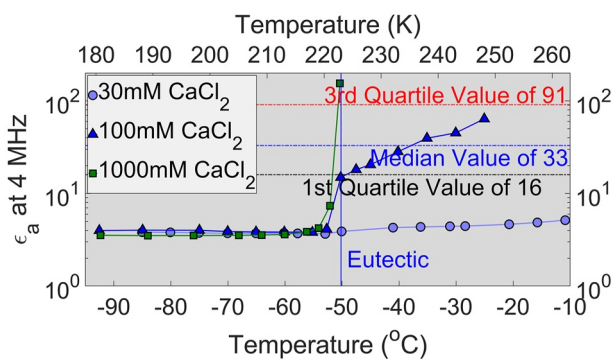

Figure 4. Apparent permittivity of various concentrations of $CaCl_2$ as a function of temperature. Of these concentrations, 100 mM (1.1 wt%) $CaCl_2$ is near the first quartile value of the observed Mars Advanced Radar for Subsurface and Ionospheric Sounding (MARSIS) ε_a at 233 K.

4.3.2. Metastability of Calcium Perchlorate

The electrical properties of perchlorate salt-H_2O mixtures and perchlorate salt-H_2O mixtures with sand were measured during freezing and warming. Magnesium perchlorate samples froze at temperatures within 10 K of their eutectic temperatures. Eight of nine calcium perchlorate samples never froze, even at for temperatures as low as163 K (24 K below the eutectic temperature), although this was not true for all experiments. We note that Toner et al. (2014) had to freeze $Ca(ClO_4)_2$–153 K before it turned to glass. The 300 mM (6.7 wt%) $Ca(ClO_4)_2$ froze at $T = 187.9$ K, but the brine remained in a metastable form down to a temperature of 187.9 ± 0.2 K, that is, 9.4 K below the eutectic. However, the measured value of ε_a is below the observed first quartile value at temperatures <189.5 K (Figure 6). The drop of ε_a with decreasing temperature (Figures 6–8) is attributed to decreasing volumes of liquid brine, combined with decreasing values of σ_{DC} at lower temperatures. A significant observation of the 300 mM (6.7 wt%) $Ca(ClO_4)_2$ is that the value of ε_a does not change whether the sample temperature is decreasing or increasing (Figure 6). This implies there is no supercooled water artificially enhancing σ_{DC} during freezing. Thus, for samples that never froze, we

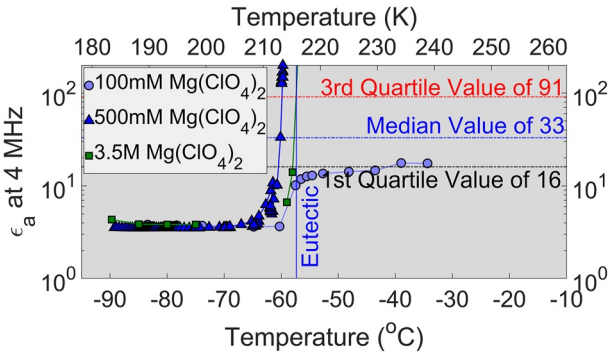

Figure 5. Apparent permittivity of various concentrations of $Mg(ClO_4)_2$ as a function of temperature. Of these concentrations, 100 mM (2.2 wt%) $Mg(ClO_4)_2$ is not able to obtain the first quartile value of the observed Mars Advanced Radar for Subsurface and Ionospheric Sounding (MARSIS) ε_a at 216 K, while 500 mM (10 wt%) and 3.5 M (44 wt%) $Mg(ClO_4)_2$ possesses an ε_a that are larger than the third quartile value above the eutectic temperature.

assume that their ε_a value at temperature at or above the eutectic temperature is consistent with a sample of the same concentration that did freeze.

Our experiments cannot determine if metastable brines are or are not stable for millions of years, but we have measured metastable $Ca(ClO_4)_2$ samples for over 72 hr, similar to previous measurements suggesting similar behavior of $MgCl_2$ (Primm et al., 2020). If brines are metastable under the SPLD, then greater concentrations of salt would be needed to match the observed MARSIS values (Figures 7 and 8). For a eutectic concentration of 3.05 M (49.8 wt%) $Ca(ClO_4)_2$ mixed with 60.2 vol% sand, a temperature >182 K is needed to obtain the values obtained the observed first quartile valves (Figure 8).

4.3.3. Calcium Perchlorate

For the 300 mM (6.9 wt%) of $Ca(ClO_4)_2$, the selected measurements of ε' (Figure 9a) and ε'' (Figure 9b) display a strong ice relaxation below the eutectic temperature. Above the eutectic temperature, σ_{DC} increases to large values (Figure 9c) so that ε' can no longer be measured accurately due to so much energy being dissipated by ε''. The observed dependence of ε_a with temperature demonstrates that concentrations of 300 mM (6.9 wt%) and 200 mM (4.7 wt%) of $Ca(ClO_4)_2$ are sufficient to obtain the observed third quartile and median value, respectively, at the measured eutectic temperature of 197.3 ± 0.2 K (Figure 9). The brine in the 200 mM (4.7 wt%) of $Ca(ClO_4)_2$ never froze into hydrate and ice even though the temperature was dropped to 161.9 K, thus only ε_a above the eutectic temperature are considered stable. The 100 mM (2.4 wt%) $Ca(ClO_4)_2$ sample also never froze and shows it is below the third quartile value.

We fit a power law to the measured data to obtain estimates of the $Ca(ClO_4)_2$-H_2O mixtures of 140 mM (3.3 wt%) and 310 mM (7.1 wt%) that match to the MARSIS observed first and third quartile values, respectively (Figure 10). The bulk brine concentrations of these concentrations at the first and third quartile values are 2.7 and 6.0 vol% at the eutectic temperature (Figure 2). Overall, $Ca(ClO_4)_2$-H_2O mixtures are a very good match for the observed MARSIS values because of its low eutectic temperature.

4.4. Salt-H_2O Mixtures in Low-Surface Area Sediments

Previous measurements (Stillman et al., 2010) have shown that brines in low-specific-surface (<1 m^2/g) area sediments also show distinct increases of σ_{DC} at the eutectic temperature that indicate that LVNs still dominate conduction in icy sediment mixtures. Our experiments were conducted with fine-grained (mean grain size of 110 μm) sand with a porosity of ~40%. We focused on $Ca(ClO_4)_2$ salt-H_2O mixture with sand. We found that a 37.8 vol% of 700 mM (15.1 wt%) $Ca(ClO_4)_2$ mixed with sand is near the observed ε_a values for the first quartile (Figure 8). Similarly, a 40.4 vol% of 1.5 mM (29.1 wt%) $Ca(ClO_4)_2$ mixed with sand is near the observed ε_a values for the median observed values (Figure 8), making this a likely material for the base of the SPLD in Ultimi Scopuli.

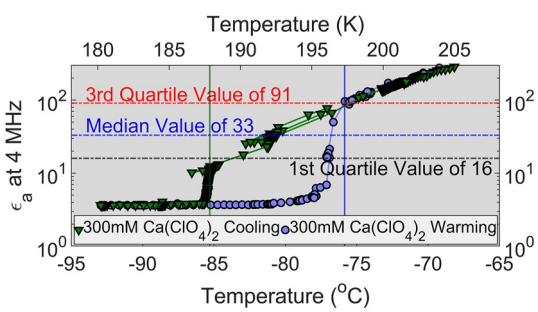

Figure 6. Apparent permittivity of 300 mM (6.9 wt%) $Ca(ClO_4)_2$ as a function of temperature for cooling and warming measurements. Note that the ε_a continues it constant decrease with temperature as it is cooled below the eutectic temperature, the brines in this sample then froze at a temperature of 187.9 K (vertical green line). Upon warming the brines then fully thaw at the eutectic temperature of 197.3 K (vertical blue line) and reach the same ε_a as during cooling.

Using a power-law fit at the eutectic temperature, we find that for a mixture that is ~60 vol% sand and 40 vol% $Ca(ClO_4)_2$-H_2O the observed ε_a values for the first and third quartile values would have a $Ca(ClO_4)_2$ concentration of 770 mM (16.4 wt%) and 2.5 M (43.4 wt%), respectively (Figure 10). We then modeled the amount of brine in the bulk sample to calculate a brine concentration of 6.3 and 28.7 vol% at the first and third quartile values, respectively.

4.5. Salt-H_2O Mixtures in High-Surface Area Sediments

Clay samples from the Clay Mineral Society were previously measured at Mars-like temperatures (Stillman et al., 2010, 2013a, 2013b). A compilation of multiple samples of STx-1 (Texas Calcium Montmorillonite) measured

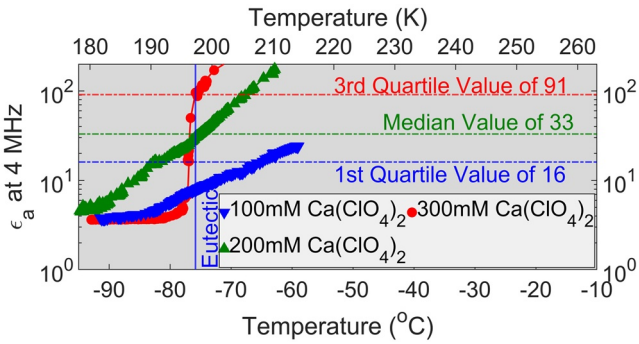

Figure 7. Apparent permittivity of mixtures as a function of temperature. The 200 mM (4.7 wt%) and 300 mM (6.9 wt%) $Ca(ClO_4)_2$ samples are near the observed median and third quartile value at temperatures greater than the eutectic, respectively. The 100 mM (2.4 wt%) $Ca(ClO_4)_2$ sample is below the first quartile value. Note the 100 and 200 mM samples never froze, thus the values below the eutectic temperature are for a metastable brine.

dry and with slight additions of water at a temperature of 193.2 ± 0.2 K are shown in Figure 11. STx-1 possesses a large H_2O surface area of 217 m^2/g (Jänchen et al., 2009), where 3 and 7 monolayers (ML) represent ∼14 and ∼32 wt% water, respectively (Note a ML of water was assumed to be 0.3 nm thick). None of the data plotted approach the ε_a threshold for the first quartile observations. Furthermore, the full temperature data set for 7 ML of 100 mM $CaCl_2$ indicates that, once the temperature drops below 233 K, the electrical properties are not compatible with the first quartile MARSIS observations (Figure 12).

For this work, we measured clay specimen SAz-1 ("Cheto" from Arizona with an N_2 surface area of 97.4 m^2/g) saturated with 54.2 wt% of 500 mM $Ca(ClO_4)_2$ brine (Figure 13). While the sample displays σ_{DC} and strong polarization mechanisms, these are not of sufficient magnitude to approach the range of ε_a values observed by MARSIS. Thus, our new experiment corroborates the conclusion that salt-H_2O mixtures in high-surface area sediments do have increased values of σ_{DC} above the eutectic temperature (Mattei et al., 2022; Stillman et al., 2010). While absorbed/bound water does conduct electrical current below and above the eutectic temperature, the ions in adsorbed/bound water are less mobile and follow a much more tortuous path compared to brines in sand or ice (Stillman et al., 2010).

JSC Mars-1, which consists of hematite and titano-magnetite, has been measured by many researchers (e.g., Stillman & Olhoeft, 2008; Williams & Greeley, 2004). When measured dry, it does not approach the first quartile values. JSC Mars-1 has a large H_2O surface area (106 m^2/g; Pommerol et al., 2009) due to a palagonitic surface. However, even with 7 ML (∼18 wt%) it still does not obtain large electrical property values approaching the range of ε_a values of that observed by MARSIS until temperatures larger than 273 K (Figure 14). In conclusion, salt-H_2O mixtures in high-surface area (>1 m^2/g) sediments do not possess a large enough σ_{DC} to provide an ε_a value at SPLD-like temperatures that is similar to the bright reflector measured by MARSIS.

5. Discussion

5.1. Dry Minerals

Shmulevich et al. (1971) measured ε', but not ε'', of intrusive and extrusive igneous rocks. Without ε'', ε_a cannot be calculated, however only 7 out of 89 have $\varepsilon' > 16$ at 500 MHz. There is little data regarding the methodology of the Shmulevich et al. (1971) measurements. Leaving many important questions: what temperature were the samples measured at, where were the samples acquired, and were the samples vacuum or thermally dried or measured as collected? Additionally, frequency and temperature dependence are also omitted. Thus, it is impossible to extrapolate these measurements to SPLD temperatures and MARSIS frequencies given the lack of details given in Shmulevich et al. (1971).

Many other measurements (Adams et al., 1996; Campbell & Ulrichs, 1969; Chung et al., 1970; Gold et al., 1970; Russell & Stasiuk, 1997) of volcanic rocks all measured $\varepsilon' < 12$ at radar frequencies. While Rust et al. (1999) found two of 34 basaltic samples, with an $\varepsilon' > 13.5$ at 4 MHz and at room temperature. Only the MB1 sample has an $\varepsilon_a > 16$ at 4 MHz at room temperature (Figure S1). Rust et al. (1999) does comments that this sample hosts thin cracks, thus a layer of absorbed water could be increasing ε' as has been measured by many other (e.g., Jonscher, 1978, 1999; Knight & Endres, 1990; Shahidi et al., 1975; Stillman et al., 2010). Thus, we are skeptical that this single basalt measurement could produce an ε_a value due to adsorbed/bound water that is larger than clay or JSC Mars-1. Overall, measurements of basalts

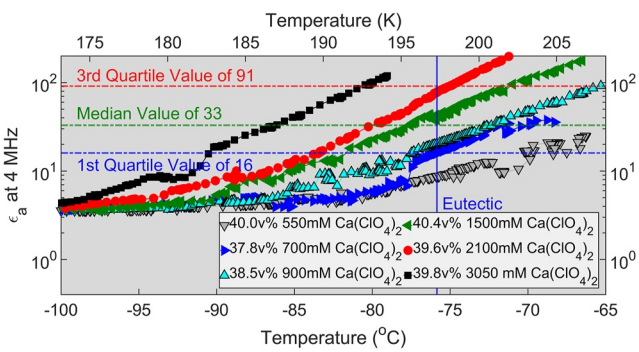

Figure 8. Fine-grained sand mixed with salt-H_2O mixtures of $Ca(ClO_4)_2$. Samples of 700 mM (15.1 wt%), 1.5 M (29.1 wt%), and 2.1 M (38.1 wt%) $Ca(ClO_4)_2$ are near the first quartile, median, and third quartile values of ε_a, respectively, at the eutectic temperature of $Ca(ClO_4)_2$. Note that the displayed data do not possess the eutectic temperature jump indicative of melting. Thus, indicating that the $Ca(ClO_4)_2$ never froze even when lowered to below 173 K. Warming cycles (shown) and the cooling cycle (not shown for simplicity) show no hysteresis, further suggesting the brine is metastable below the eutectic temperature.

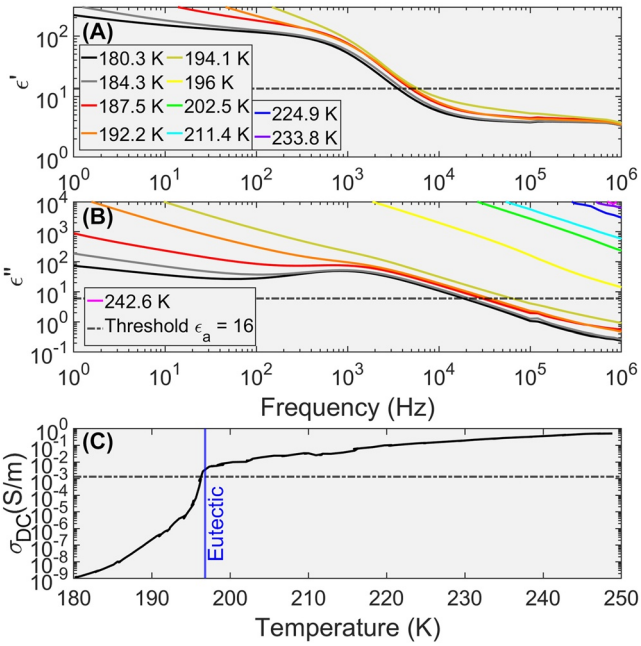

Figure 9. Real (a) and imaginary (b) part of the relative permittivity, and modeled Direct Current (DC) conductivity (c) of 300 mM (6.9 wt%) $Ca(ClO_4)_2$ as a function of temperature. (a) and (b) Show spectrum at selected temperatures, while (c) shows all the spectrum fitted over the entire measurement run. Note below the eutectic temperature the sample shows a dielectric relaxation of ice, however once the eutectic is reached the sample becomes conductive and ε' is not shown as it has little accuracy as all the energy is being dissipated conductively.

do not appear to be capable of reaching the observed first quartile values. However, more measurements of various dry basalt at cold temperatures should be conducted to ensure that none can obtain ε_a values consistent with the observed first quartile values.

Gray hematite possesses a radio-frequency relaxation with a small activation energy of 0.1 eV (Stillman & Olhoeft, 2008). A dry sample of 59.0 vol% gray hematite with a porosity of 41.0% can obtain the median observed MARSIS ε_a value at 4 MHz over possible SPLD-like temperatures (Figure 15). This is a significant amount of gray hematite and about four times greater than the maximum gray hematite value measured at the surface of 15% at Aram Chaos and Meridiani Planum (Glotch & Christensen, 2005). Additionally, the gray hematite in Meridiani Planum is a lag deposit and thus concentrated compared to its in situ formation concentration (Hynek, 2004). This is likely why no large increases in surface reflectivity have been measured at Aram Chaos or Meridiani Planum even though they have a high surficial concentration of gray hematite.

To further explore the possibilities of gray hematite, we perform dielectric mixing models. Using a Licktenecker power law mixing formula (Stillman & Olhoeft, 2008), we estimate the solid grain ε_a of gray hematite to be 137.6 at 4 MHz at 200 K, assuming a grain density δ_G of 5.26 g cm^{-3}. We then used Equation 1 to estimate an ε_a value of ultramafic and mafic grain assuming a δ_G of 3.8 and 3.0 g cm^{-3}, respectively. We assume that any porosity is filled with ice (no brine) with ε_a of 3.15 as ground ice is stable below the SPLD. We then created four mixing models with gray hematite (Figure 16; Table 1) using a power-law mixing model with an exponent of 2.65 (Shabtaie & Bentley, 1994; Stillman et al., 2010). First, we mix gray hematite with ice that produces gray hematite volume concentrations of 26.8%–45.2%–81.0% for the observed first quartile-median-third quartile values. The replacement of the porosity with ice reduces the volume concentration of the median value from 59.0% (Figure 16) to 45.2%, however this is still three times larger than the largest values detected on the surface of Mars. We then assume an ice-filled porosity of 19% and 10%, while mixing the ultramafic grains with gray hematite. This produces smaller gray hematite concentrations of 12.4%–35.6%–81.0% and 10.0%–33.2%–78.6% for ice concentrations of 19% and 10%, respectively, for the observed first quartile-median-third values. These values of gray hematite are only about two times larger than those detected on the surface, however the bulk density δ_B of these mixtures are higher than any typical volcanic rocks measured on Earth (Kiefer et al., 2012; Olhoeft & Johnson, 1984; Rust et al., 1999; Shmulevich et al., 1971). To reduce δ_B, we then mixed a 10% ice with gray hematite and mafic grains to produce gray hematite concentrations of 18.5%–39.2%–79.8%. Such a reduction in δ_B leads to an increase in gray hematite concentration, and would likely still produce a measurable gravity anomaly. Li et al. (2012) displays no gravity anomaly is present at the Ultimi Scopuli site, albeit greater gravity resolution is needed before this could be totally ruled out. Overall, we find that large amounts of gray hematite can create ε_a values that match the MARSIS observations. However, the concentration of gray hematite (median values from 33.2 to 59.0 vol% and third quartile value from 78.6 to 81.0 vol%) and extent (20–30 km ellipse) of the deposits needed rival that of terrestrial banded iron formation, such formations are not expected on Mars.

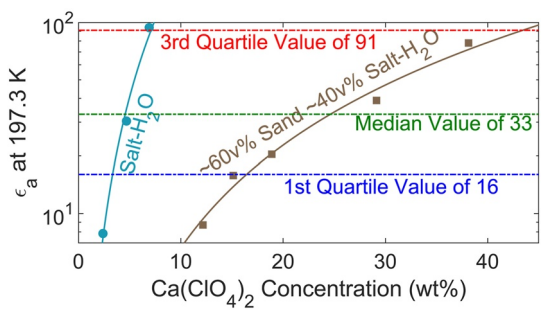

Figure 10. Apparent permittivity at the eutectic temperature versus calcium perchlorate mass concentration. The three experiments (symbols) of the salt-H_2O mixtures were fit (solid line) with a power law to calculate the first quartile, median, and third quartile values of 3.3, 4.6, and 7.1 wt%, respectively. The five experiments of the sand mixtures with salt-H_2O were similarly fit with a power law to calculate the first quartile, median, and third quartile values of 16.4, 24.6, and 43.4 wt%, respectively.

5.2. Metastability

Measurements made while cooling brine mixtures can show significant hysteresis as well as long-term (of at least a few days) stability even when mixed with sand (Figures 6–8; Primm et al., 2020). Unlike the measurements

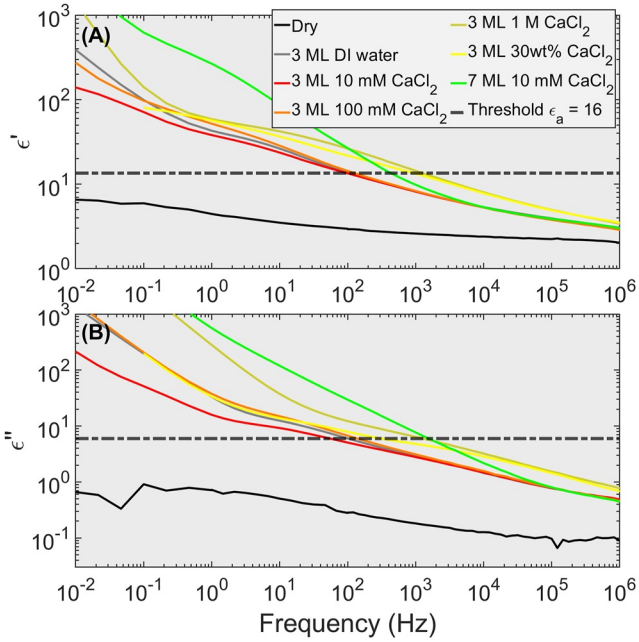

Figure 11. Compilation of ε' (a) and ε'' (b) values of dry and low-saturation measurements of Texas Calcium Montmorillonite (STx-1) at ~193.2 ± 0.2 K, where ML is the number of calculated monolayers. At this temperature, the samples show no enhanced ε' or ε'' that could explain the Mars Advanced Radar for Subsurface and Ionospheric Sounding (MARSIS) observed values measurements.

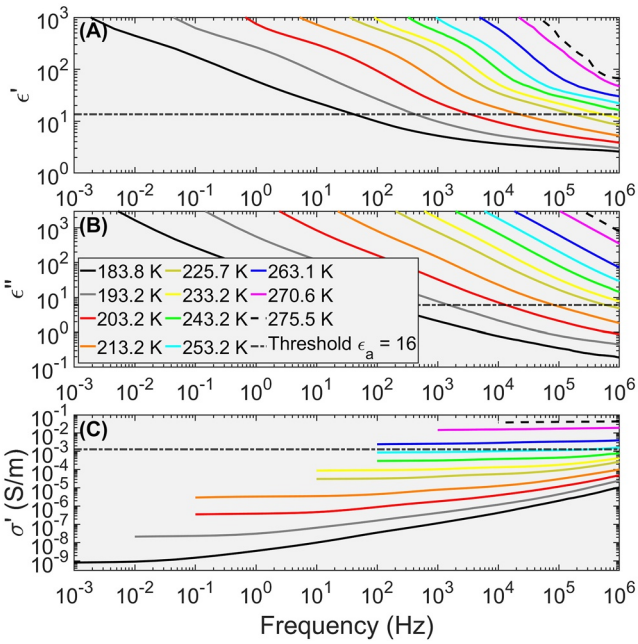

Figure 12. STx-1 measurements with 7 ML 100 mM (1.1 wt%) $CaCl_2$ for ε' (a), ε'' (b), and σ' (c). This sample had a STx-1, 100 mM $CaCl_2$, and air mass (volume) concentration of 70.4 mass% (28.0 vol%), 29.6 mass% (32.4 vol%), and 0 mass% (39.6 vol%), respectively. At 1 MHz, the electrical properties cannot obtain the ε_a threshold when temperatures are <233 K.

of $MgCl_2$ (Primm et al., 2020), we could not reproduce the metastability of $Ca(ClO_4)_2$. One $Ca(ClO_4)_2$ experiment froze at 188 K, while seven other experiments it did not freeze down to ~173 K and in one case down to 161.9 K. This behavior is consistent with Toner et al. (2014) where two $Ca(ClO_4)_2$ samples did not freeze until 153 K. It is far from demonstrated that the longevity of metastable brine shown in laboratory settings extends over geologic timescales. Therefore, we ignore metastable effects until future improved temperature models can fully eliminate the possibility of SPLD basal temperatures of 197.3 K.

5.3. Brine Mixtures

To match the MARSIS observed values, brine concentrations of 2.7–6.0 vol% and 6.3–28.7 vol% for salt-H_2O and salt-H_2O-sediment mixtures, respectively, are necessary (Figure 10). In salt-H_2O-sediment mixtures, the salt-H_2O just occupies the pore space. Thus, a greater concentration of salt is needed when mixed with sediment to match the MARSIS observations compared to the salt-H_2O mixtures without sediment. Thus, we find that the brine concentration in fine sand must be 2–5 times larger than when the brine is just in ice. This occurs because of increased tortuosity of the LVNs, which leads to a lower σ_{DC}. This drop in σ_{DC} is much larger when the pores and pore throats are even smaller. Therefore, high-specific surface area sediments (i.e., clays and JSC Mars-1) possess LVNs, but with high tortuosity and small σ_{DC} (Stillman et al., 2010; Stillman et al., 2013b; Stillman et al., 2013a, Figures 11–14) Thus, these salt-H_2O-sediment mixtures cannot obtain the MARSIS observed ε_a values.

5.4. Salt Enhancement

The salt-regolith concentration discovered at the Phoenix landing site was 0.7 mass% (Hecht et al., 2009). Our first quartile, median, and third quartile salt-H_2O-sediment values have a salt-bulk sample concentration of 3.6, 5.7, and 11.3 mass%, respectively. Thus, the sediment at the basal layer of the SPLD would have to be enhanced by a factor of ~5–16 compared to the Phoenix landing site. We are considering two salt enhancement mechanisms as theoretically possible:

1. Drainage of an interconnected system of LVNs that would concentrate brines downward through a deposit, such as the SPLD. This process has been observed, for example, in temperate sea-ice (e.g., Nye & Frank, 1973) and has been hypothesized to occur within the Europa ice shell (e.g., Hesse et al., 2022).
2. Sublimation of CO_2/H_2O snow or ice due to changes in orbital parameters can concentrate the amount of dust. Indeed, images of the regions surrounding the SPLD show layers with varying amount of dust (some likely with more than 10%; Milkovich & Plaut, 2008). Perhaps a similar mechanism might be responsible for salt enrichment in the upper layers of the regolith, as for example, observed in the upper dry valleys of Antarctica where, when snow sublimates, leaves behind salt-enriched sediments (Levy et al., 2012).

5.5. Implications

The question of the source of the bright basal reflections observed by MARSIS in Ultimi Scopuli has generated significant debate (Schroeder &

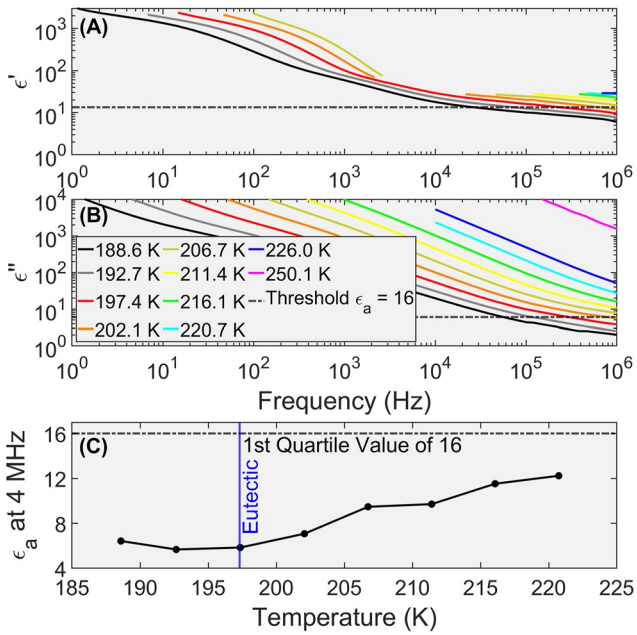

Figure 13. Complex electrical property measurements SAz-1 saturated with 500 mM (11.2 wt%) $Ca(ClO_4)_2$ with a mass (volume) concentration of 45.8 mass% (25.5 vol%) sand and 54.2 mass% (74.5 vol%) of salt-H_2O. (a) ε', (b) ε'', and (c) ε_a of the mixture shows that the sample has low-frequency broad dielectric relaxations and high Direct Current (DC) conductivity, but never approaches the observed first quartile value.

Steinbrügge, 2021). On one side, perchlorate brines are not expected to be liquid at the values of basal temperatures commonly reported in the literature (e.g., Egea-Gonzáles et al., 2022; Sori & Bramson, 2019). All other types of materials thus far proposed as possible reflectors (Bierson et al., 2021; Grima et al., 2022; Smith et al., 2021), however, have not stood the test of laboratory experiments (Mattei et al., 2022). In the experimental work reported here, we have expanded the types of materials and tested their dielectric properties over a broad range of temperatures, showing that liquid brines and gray hematite are the only materials with a dielectric response consistent with MARSIS observations. To explain the bright basal reflections, however, the quantity of gray hematite at the base of the SPLD should be 2–3 times that observed at Meridiani Planum, which appears geologically unlikely. For brines, we need to work out whether it is possible that basal temperatures are indeed higher than previously thought, for example, by addition of low-conductivity layers (e.g., CO_2 ice), or consider metastability.

The fact that metastable perchlorate brines are known to exist at temperatures well below those of their eutectics in the laboratory (e.g., Toner et al., 2014; Primm et al., 2017, 2020; and the experiments reported here), provides a clear direction for future work. Nevertheless, it is difficult to envisage conditions of metastability that persist at geological timescales. Thus, renewed efforts must be made to investigate the specific set of physical and geological conditions that may have led to the formation of the brines and to their preservation through time.

It is generally accepted that cyclical variations of Mars's orbital parameters influenced climate cycles as recorded in the polar caps (e.g., Laskar et al., 2004). The Noachian crust underlaying the south polar cap is very

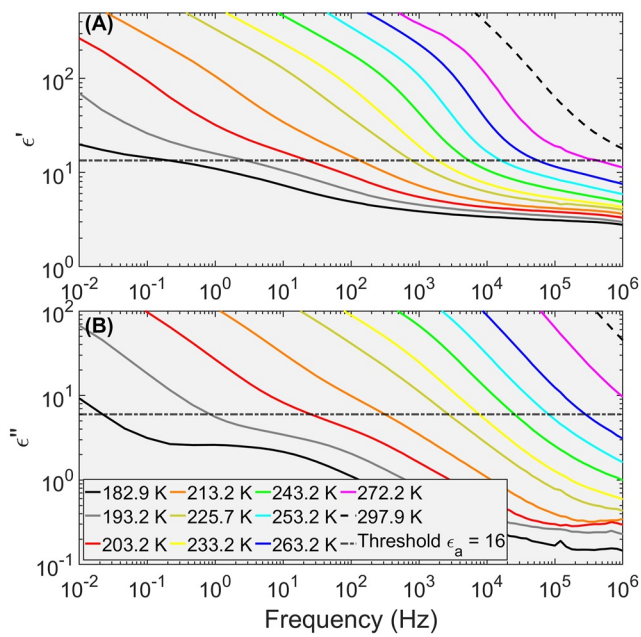

Figure 14. Complex electrical property measurements of JSC Mars-1 with 7 ML of 100 mM (1.1 wt%) $CaCl_2$. JSC Mars-1, 100 mM $CaCl_2$, and air in this partially-saturated sample had a mass (volume) concentration of 82.2 mass% (43.3 vol%), 17.8 mass% (17.9 vol%), and 0 mass% (38.8 vol%), respectively. The electrical properties do not approach the ε_a threshold for the first quartile value until the sample becomes completely unfrozen (>273 K). Thus, even with multiple polarization mechanisms of adsorbed water and ice combined with Direct Current (DC) conductivity cannot approach the observed Mars Advanced Radar for Subsurface and Ionospheric Sounding (MARSIS) threshold.

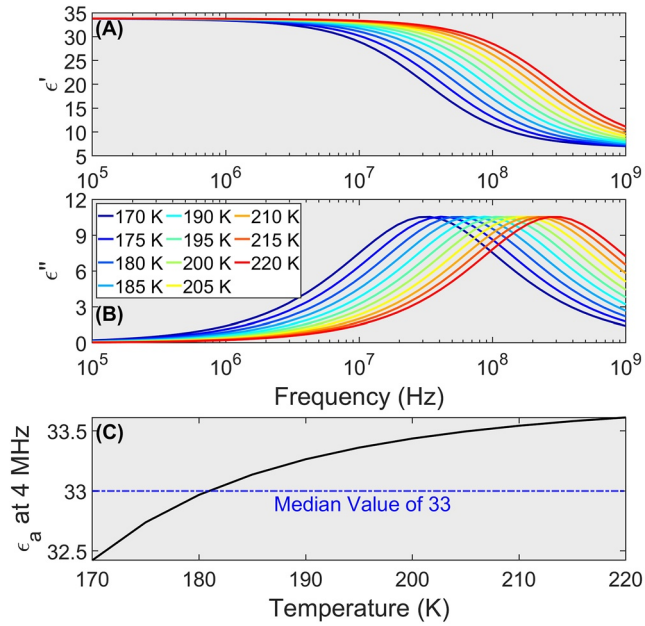

Figure 15. Electrical properties of gray hematite based on radar measurements modeled by Stillman and Olhoeft (2008). Note this model represent the measured sample that had a porosity of 41% and a gray hematite volume concentration of 59%. This high-frequency relaxation does not greatly affect ε_a at 4 MHz over typical South Polar Layered Deposits (SPLD) temperatures.

different from that presently covered by the north polar cap, which is much younger in age (late Amazonian). The south polar region is also approximately 7–8 km higher in elevation than the north polar region. Since no bright radar reflections have been observed in the north, it is plausible that a combination of peculiar geographic and geological conditions may be responsible for the presence of basal liquid brines in the south. The geologic setting of the areas surrounding the SPLD has been studied in detail through interpretation of geomorphological features (e.g., Butcher et al., 2016; Dickson & Head, 2006; Ghatan & Head, 2002; Guallini et al., 2018; Kress & Head, 2015; Scanlon et al., 2018), and a geological context for the surface of the SPLD at Ultimi Scopuli has recently been published (Landis & Whitten, 2022).

Future efforts need to reconcile surface observations with spatial and temporal reconstructions of the sequence of geological events at Ultimi Scopuli, interpreted within a broader astronomical perspective linked to climate variations. This will contribute to elucidate the specific large-scale conditions that make the location suitable for the accumulation of liquid brines. In parallel, the physical parameters of processes at micro- and mesoscale, involving the segregation of liquid and solid phases at the grain boundaries of impurities in the SPLD, must be specifically investigated, with a focus on non-equilibrium conditions that might explain how hypersaline aqueous solutions can persist at sub-eutectic temperatures. Upon completion of these studies, the liquid brines at the base of the SPLD should be viewed as an additional data-point in the global reconstruction of the evolution of Mars and of its climate history.

6. Conclusions

We compiled new and old measurements of electrical properties of Martian analog materials at SPLD basal temperatures. In this paper, we have shown that of all the materials proposed as the source of the bright reflections at Ultimi Scopuli, brine-rich ice mixtures are the most viable option. Because they have the lowest eutectic temperature of any common Martian salt, $Ca(ClO_4)_2$ brines are most likely. The concentration of $Ca(ClO_4)_2$ to H_2O needed is 140–310 mM (3.3–7.1 mass%) to obtain the observed ε_a first and third quartile values. Likewise if liquid brines exist in sediment with ~40% porosity, a larger concentration of 0.77–2.5 M (16.4–43.4 mass%) of $Ca(ClO_4)_2$ is required to obtain the observed first and third quartile values. Thus, the sediments require ~5–16 times the concentration of salt measured at the Phoenix landing site. However, $Ca(ClO_4)_2$ brines are only stable

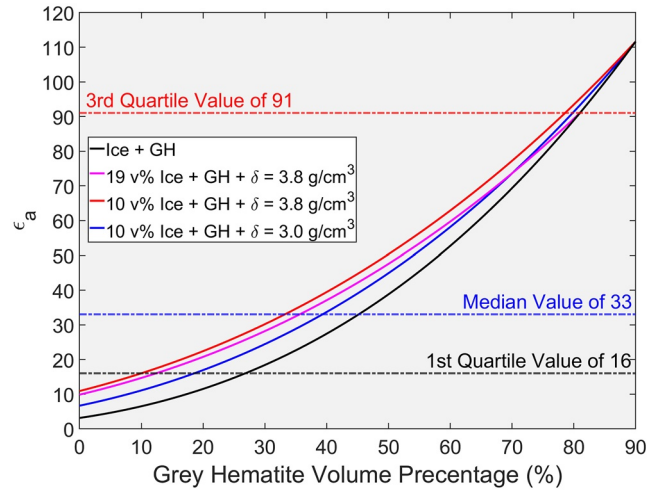

Figure 16. Four gray hematite (GH) mixing models are used to estimate the concentrations of ice, GH at 200 K, ultramafic (density $\delta = 3.8$ g cm^{-3}) and mafic ($\delta = 3.0$ g cm^{-3}) grains that would match the observed Mars Advanced Radar for Subsurface and Ionospheric Sounding (MARSIS) ε_a values. Precise values are given in Table 1.

above its measured eutectic temperature of 197.3 ± 0.2 K, which is higher than the estimates of simple SPLD thermal models. It is possible that low-conductivity material layers mixed in with H_2O in the deposits could modify the thermal gradient and thus result in basal temperatures above the $Ca(ClO_4)_2$ eutectic. The volume of brine is estimated to be 2.7–6.0 vol% and 6.3–28.7 vol% in ice mixtures and sand mixed ice, respectively. Thus,

Table 1
Values of the Four Gray Hematite (GH) Mixing Models Shown in Figure 15 at the Observed First and Third Quartile and Median Values of ε_a

ε_a	Ice	GH	$\delta_G = 3.8$ g cm^{-3}	$\delta_G = 3.0$ g cm^{-3}	δ_B g cm^{-3}	δ_B g cm^{-3} when replace ice with air	Comments
91	19.0%	81.0%			4.43	4.26	High density; Significant vol% of GH
33	54.8%	45.2%			2.87	2.37	Significant vol% of GH
16	73.2%	26.8%			2.08	1.41	Possible
91	19.0%	81.0%	0.0%		4.43	4.26	High density; Significant vol% of GH
33	19.0%	35.6%	45.4%		3.77	3.60	High density; Significant vol% of GH
16	19.0%	12.4%	68.6%		3.43	3.26	Possible
91	10.0%	78.6%	11.4%		4.66	4.57	High density; Significant vol% of GH
33	10.0%	33.2%	56.8%		4.00	3.90	High density; Significant vol% of GH
16	10.0%	10.0%	80.0%		3.66	3.57	High density
91	10.0%	79.8%		10.2%	4.59	4.50	High density; Significant vol% of GH
33	10.0%	39.2%		50.8%	3.68	3.59	High density; Significant vol% of GH
16	10.0%	18.5%		71.5%	3.21	3.12	Possible

Note. The grain density δ_G values of 3.8 and 3.0 g cm^{-3} were used to represent an ultramafic and mafic grain density, respectively, and converted to permittivity using Equation 1. A δ_G of 5.26 and 0.917 g cm^{-3} were used for GH and ice, respectively, to calculate the bulk density δ_B. Note we assume that all pore space is filled by ice as ground ice should be stable under the SPLD. We also calculate δ_B by neglecting the contribution of ice to allow us to compare to terrestrial δ_B of rocks. In the comment's column, we assume that any rocks with a δ_B larger than 3.5 g cm^{-3} are too high (the largest density of the volcanic samples measured by Rust et al. (1999) and Shmulevich et al. (1971) was a gabbro at 3.39 g cm^{-3}). Additionally, we commented that any solution with a GH concentration greater than 30 vol% was too large as Thermal Emission Spectrometer spectroscopic observations detected a maximum of 15 vol% of GH over Aram Chaos and Meridiani Planum (Glotch & Christensen, 2005).

partially-saturated ice or ice-sediment mixtures could produce the observed reflection. Unprocessed MARSIS data were key to detect the bright basal reflections in Ultimi Scopuli. More work is required in this area, to search for other anomalous regions of high reflectivity in order to determine whether Ultimi Scopuli is unique, or just the largest of many similar features. By acquiring a large number of "data-points" we will also be able to narrow the possible mechanisms leading to salt enhancement.

Data Availability Statement

Data for this paper can be found in Stillman (2022).

Acknowledgments
The authors thank Editor B. Thompson and two anonymous reviewers whose constructive comments improved the explanation and discussion of the findings. We acknowledge the support of the space agencies of Italy (ASI) and the United States (NASA) for the development and science operations of MARSIS. Operations of the Mars Express spacecraft by the European Space Agency (ESA) are gratefully acknowledged. D.S. was supported by NASA Grant 80NSSC20K0858. The authors thank Luca Guallini, Francesco Soldovieri, and Robert Grimm for intellectual discussions regarding this subject. D.S. thanks Michael Shoffner for his laboratory assistance.

References

Adams, R. J., Perger, W. F., Rose, W. I., & Kostinski, A. (1996). Measurements of the complex dielectric constant of volcanic ash from 4 to 19 GHz. *Journal of Geophysical Research*, *1*(B4), 8175–8185. https://doi.org/10.1029/96jb00193

Bierson, C. J., Tulaczyk, S., Courville, S. W., & Putzig, N. E. (2021). Strong MARSIS radar reflections from the base of Martian south polar cap may be due to conductive ice or minerals. *Geophysical Research Letters,* 48*(*13), e2021GL093880. https://doi.org/10.1029/2021gl093880

Butcher, F. E. G., Conway, S. J., & Arnold, N. S. (2016). Are the dorsa argentea on Mars eskers? *Icarus*, *275*, 65–84. https://doi.org/10.1016/j.icarus.2016.03.028

Campbell, M. J., & Ulrichs, J. (1969). Electrical properties of rocks and their significance for lunar radar observations. *Journal of Geophysical Research*, *25*, 5867–5881. https://doi.org/10.1029/jb074i025p05867

Chung, D. H., Westphal, W. B., & Simmons, G. (1970). Dielectric properties of Apollo 11 lunar samples and their comparison with Earth materials. *Journal of Geophysical Research*, *75*(32), 6524–6531. https://doi.org/10.1029/jb075i032p06524

Cole, K. S., & Cole, R. H. (1941). Dispersion and absorption in dielectrics. *The Journal of Chemical Physics*, *9*(4), 341–351. https://doi.org/10.1063/1.1750906

Cunje, A. B., Ghent, R. R., Boivin, A., Tsai, C. A., & Hickson, D. (2018). Dielectric properties of Martian regolith analogs and smectite clays. *Lunar and Planetary Science Conference*, 2083.

Dickson, J., & Head, J. W. (2006). Evidence for an Hesperian-aged south circum-polar lake margin environment on Mars. *Planetary and Space Science*, *54*(3), 251–272. https://doi.org/10.1016/j.pss.2005.12.010

Egea-González, I., Lois, P. C., Jiménez-Díaz, A., Bramson, A. M., Sori, M. M., Tendero-Ventanas, J. A., & Ruiz, J. (2022). The stability of a liquid-water body below the south polar cap of Mars. *Icarus*, *383*, 115073. https://doi.org/10.1016/j.icarus.2022.115073

Ghatan, G. J., & Head, J. W. (2002). Candidate subglacial volcanoes in the south polar region of Mars: Morphology, morphometry and eruption conditions. *Journal of Geophysical Research: Planets*, *107*(E7), 5048. https://doi.org/10.1029/2001JE001519

Glotch, T. D., & Christensen, P. R. (2005). Geologic and mineralogic mapping of Aram Chaos: Evidence for a water-rich history. *Journal of Geophysical Research*, *110*(E9), E09006. https://doi.org/10.1029/2004JE002389

Gold, T., Campbell, M. J., & O'Leary, B. T. (1970). Optical and high-frequency electrical properties of the lunar sample. *Science*, *167*(3918), 707–709. https://doi.org/10.1126/science.167.3918.707

Grima, C., Mouginot, J., Kofman, W., Hérique, A., & Beck, P. (2022). The basal detectability of an ice-covered Mars by MARSIS. *Geophysical Research Letters*, *49*(2), e2021GL096518. https://doi.org/10.1029/2021GL096518

Grimm, R. E., Stillman, D. E., Dec, S. F., & Bullock, M. A. (2008). Low-frequency electrical properties of polycrystalline saline ice and salt hydrates. *Journal of Physical Chemistry*, *B112*(48), 15382–15390. https://doi.org/10.1021/jp8055366

Gross, G. W., Wong, P. M., & Humes, K. (1977). Concentration dependent solute redistribution at the ice-water phase boundary. III. Spontaneous convection. Chloride solutions. *Journal of Chemical Physics*, *67*(11), 5264–5274. https://doi.org/10.1063/1.434704

Guallini, L., Rossi, A. P., Forget, F., Marinangeli, L., Lauro, S. E., Pettinelli, E., et al. (2018). Regional stratigraphy of the South polar layered deposits (Promethei Lingula, Mars): "Discontinuity-bounded" units in images and radagrams. *Icarus*, *308*, 76–107. https://doi.org/10.1016/j.icarus.2017.08.030

Hecht, M. H., Kounaves, S. P., Quinn, R. C., West, S. J., Young, S. M. M., Ming, D. W., et al. (2009). Detection of perchlorate and the soluble chemistry of Martian soil at the phoenix lander site. *Science*, *325*(5936), 64–67. https://doi.org/10.1126/science.1172466

Hesse, M. A., Jordan, J. S., Vance, S. D., & Oza, A. V. (2022). Downward oxidant transport through Europa's ice shell by density-driven brine percolation. *Geophysical Research Letters*, *49*(5), e2021GL095416. https://doi.org/10.1029/2021GL095416

Hynek, B. (2004). Implications for hydrologic processes on Mars from extensive bedrock outcrops throughout Terra Meridiani. *Nature*, *431*(7005), 156–159. https://doi.org/10.1038/nature02902

Jänchen, J., Bish, D. L., & Hellwig, U. (2009). The H2O sorption properties of a Martian dust analog. In *40th lunar and planetary science conference*.1395.

Jonscher, A. K. (1978). Low-frequency dispersion in carrier-dominated dielectrics. *Philosophical Magazine B: Physics of Condensed Matter: Statistical Mechanics, Electronic, Optical and Magnetic Properties*, *38*(6), 587–601. https://doi.org/10.1080/13642817808246336

Jonscher, A. K. (1999). Dielectric relaxation in solids. *Journal of Physics D Applied Physics*, *32*(14), R57–R70. https://doi.org/10.1088/0022-3727/32/14/201

Khan, A., Ceylan, S., van Driel, M., Giardini, D., Lognonné, P., Samuel, H., et al. (2021). Upper mantle structure of Mars from InSight seismic data. *Science*, *373*(6553), 434–438. https://doi.org/10.1126/science.abf2966

Kiefer, W. S., Macke, R. J., Britt, D. T., Irving, A. J., & Consolmagno, G. J. (2012). The density and porosityof lunar rocks. *Geophysical Research Letters*, *39*(7), L07201. https://doi.org/10.1029/2012GL051319

Knight, R. J., & Endres, A. (1990). A new concept in modeling the dielectric response of sandstones: Defining a wetted rock and bulk water system. *Geophysics*, *55*(5), 586–594. https://doi.org/10.1190/1.1442870

Kress, A. M., & Head, J. W. (2015). Late noachian and early hesperian ridge systems in the South circumpolar dorsa argentea formation, Mars: Evidence for two stages of melting of an extensive late noachian ice sheet. *Planetary and Space Science*, *109–110*, 1–20. https://doi.org/10.1016/j.pss.2014.11.025

Kułacz, K., & Orzechowski, K. (2019). Nontronite and intercalated nontronite as effective and cheap absorbers of electromagnetic radiation. *Dalton Transactions*, *48*(12), 3874–3882. https://doi.org/10.1039/c9dt00132h

Landis, M. E., & Whitten, J. L. (2022). Geologic context of the bright MARSIS reflectors in Ultimi Scopuli, South Polar Layered Deposits, Mars. *Geophysical Research Letters*, *49*, e2022GL098724. https://doi.org/10.1029/2022GL098724

Laskar, J., Correia, A. C. M., Gastineau, M., Joutel, F., Levrard, B., & Robutel, P. (2004). Long term evolution and chaotic diffusion of the insolation quantities of Mars. *Icarus*, *170*(2), 343–364. https://doi.org/10.1016/j.icarus.2004.04.005

Lauro, S. E., Pettinelli, E., Caprarelli, G., Guallini, L., Rossi, A. P., Mattei, E., et al. (2021). Multiple subglacial water bodies below the south pole of Mars unveiled by new MARSIS data. *Nature Astronomy*, *5*(1), 63–70. https://doi.org/10.1038/s41550-020-1200-6

Levy, J. S., Fountain, A. G., Welch, K. A., & Lyons, W. B. (2012). Hypersaline "wet patches" in Taylor valley, Antarctica. *Geophysical Research Letters*, *39*(5), L05402. https://doi.org/10.1029/2012GL050898

Li, J., Andrews-Hanna, J. C., Sun, Y., Phillips, R. J., Plaut, J. J., & Zuber, M. T. (2012). Density variations within the south polar layered deposits of Mars. *Journal of Geophysical Research*, *117*(E4), E04006. https://doi.org/10.1029/2011JE003937

Lorek, A., & Wagner, N. (2013). Supercooled interfacial water in fine-grained soils probed by dielectric spectroscopy. *The Cryosphere*, *7*(6), 1839–1855. https://doi.org/10.5194/tc-7-1839-2013

Mattei, E., Pettinelli, E., Lauro, S. E., Stillman, D. E., Cosciotti, B., Marinangeli, L., et al. (2022). Assessing the role of clay and salts on the origin of MARSIS basal bright reflections at Ultimi Scopuli, Mars. *Earth and Planetary Science Letters*, *579*, 117370. https://doi.org/10.1016/j.epsl.2022.117370

Mellon, M. T. (1996). Limits on the CO2 content of the Martian polar deposits. *Icarus*, *124*(1), 268–279. https://doi.org/10.1006/icar.1996.0203

Milkovich, S. M., & Plaut, J. J. (2008). Martian south polar layered deposit stratigraphy and implications for accumulation history. *Journal of Geophysical Research*, *113*(E6), E06007. https://doi.org/10.1029/2007JE002987

Moore, J. C., & Maeno, N. (1993). Dielectric properties of frozen clay and silt soils. *Cold Regions Science and Technology*, *21*(3), 265–273. https://doi.org/10.1016/0165-232x(93)90070-o

Nye, J. F., & Frank, F. C. (1973). Hydrology of the intergranular veins in a temerate glacier. In *Symposium on the Hydrology of Glaciers* (Vol. 95). Cambridge England.

Ojha, L., Karimi, S., Buffo, J., Nerozzi, S., Holt, J. W., Smrekar, S., & Chevrier, V. (2021). Martian mantle heat flow estimate from the lack of lithospheric flexure in the south pole of Mars: Implications for planetary evolution and basal melting. *Geophysical Research Letters*, *48*, e2020GL091409. https://doi.org/10.1029/2020GL091409

Olhoeft, G. R., & Johnson, G. R. (1984). In R. S. Carmichael (Ed.), *Handbook of physical properties of rocks* (Vol. III). CRC Press, Inc.

Olhoeft, G. R., & Strangway, D. W. (1975). Electrical properties of the first 100 meters of the moon. *Earth and Planetary Science Letters*, *24*(3), 394–404. https://doi.org/10.1016/0012-821x(75)90146-6

Orosei, R., Lauro, S. E., Pettinelli, E., Cicchetti, A., Coradini, M., Cosciotti, B., et al. (2018). Radar evidence of subglacial liquid water on Mars. *Science*, *361*(6401), 490–493. https://doi.org/10.1126/science.aar7268

Parkhomenko, E. I. (1967). Electrical properties of rocks.

Parro, L. M., Jiménez-Díaz, A., Mansilla, F., & Ruiz, J. (2017). Present-day heat flow model of Mars. *Nature Scientific Reports*, *7*(1), 45629. https://doi.org/10.1038/srep45629

Petrenko, V. F., & Whitworth, R. W. (1999). *Physics of ice* (1st ed.). Oxford Univercity Press.

Picardi, G., Plaut, J. J., Biccari, D., Bombaci, O., Calabrese, D., Cartacci, M., et al. (2005). Radar sounding of the subsurface of the Mars. *Science*, *310*(5756), 1925–1928. https://doi.org/10.1126/science.1122165

Pommerol, A., Schmitt, B., Beck, P., & Brissaud, O. (2009). Water sorption on Martian regolith analogs: Thermodynamics and near-infrared reflectance spectroscopy. *Icarus*, *204*(1), 114–136. https://doi.org/10.1016/j.icarus.2009.06.013

Primm, K. M., Gough, R. V., Chevrier, V. F., & Tolbert, M. A. (2017). Freezing of perchlorate and chloride brines under Mars-relevant conditions. *Geochimica et Cosmochimica Acta*, *212*, 211–220. https://doi.org/10.1016/j.gca.2017.06.012

Primm, K. M., Stillman, D. E., & Michaels, T. I. (2020). Investigating the hysteretic behavior of Mars-relevant chlorides. *Icarus*, *342*, 113342. https://doi.org/10.1016/j.icarus.2019.06.003

Robinson, D. A., & Friedman, S. P. (2003). A method for measuring the solid particle permittivity or electrical conductivity of rocks, sediments, and granular materials. *Journal of Geophysical Research*, *108*(B2), 2076. https://doi.org/10.1029/2001JB000691

Russell, J. K., & Stasiuk, M. V. (1997). Characterization of volcanic deposits with ground penetrating radar. *Bulletin of Volcanology*, *58*(7), 515–527. https://doi.org/10.1007/s004450050159

Rust, A., Russell, J., & Knight, R. (1999). Dielectric constant as a predictor of porosity in dry volcanic rocks. *Journal of Volcanology and Geothermal Research*, *91*(1), 79–96. https://doi.org/10.1016/s0377-0273(99)00055-4

Scanlon, K. E., Head, J. W., Fastook, J. L., & Wordsworth, R. D. (2018). The dorsa argentea formation and the noachian-hesperian climate transition. *Icarus*, *299*, 339–363. https://doi.org/10.1016/j.icarus.2017.07.031

Schroeder, D. M., & Steinbrügge, G. (2021). Alternatives to liquid water beneath the south polar ice cap of Mars. *Geophysical Research Letters*, *48*(19), e2021GL095912. https://doi.org/10.1029/2021GL095912

Shabtaie, S., & Bentley, C. R. (1994). Unified theory of electrical conduction in firn and ice: Site percolation and conduction in snow and firn. *Journal of Geophysical Research*, *99*(B10), 19757–19769. https://doi.org/10.1029/94jb01510

Shahidi, M., Hasted, J. B., & Jonscher, A. K. (1975). Electrical Properties of dry and humid sand. *Nature*, *258*(5536), 595–597. https://doi.org/10.1038/258595a0

Shmulevich, S. A., Troitskiy, V. S., Zelinskaya, M. R., Markov, M. S., & Sukhanov, A. L. (1971). Dielectric properties of rocks at a frequency of 500 MHz. *Earth Physics*, *12*, 68–76.

Smith, I. B., Lalich, D., Rezza, C., Horgan, B., Whitten, J. L., Nerozzi, S., & Holt, J. W. (2021). A solid interpretation of bright radar reflectors under the Mars south polar ice. *Geophysical Research Letters*, *48*(15), e2021GL093618. https://doi.org/10.1029/2021gl093618

Sori, M. M., & Bramson, A. M. (2019). Water on Mars, with a grain of salt: Local heat anomalies are required for basal melting of ice at the South pole today. *Geophysical Research Letters*, *46*(3), 1222–1231. https://doi.org/10.1029/2018gl080985

Stillman, D. (2022). Partially-saturated brines within basal ice or sediments can explain the bright basal reflections in the south polar layered deposits (Version 1) [Dataset]. Zenodo. https://doi.org/10.5281/ZENODO.6600729

Stillman, D., & Olhoeft, G. (2008). Frequency and temperature dependence in electro-magnetic properties of Martian analog minerals. *Journal of Geophysical Research: Planets*, *113*(E9), E09005. https://doi.org/10.1029/2007je002977

Stillman, D. E., & Grimm, R. E. (2011a). Dielectric signatures of adsorbed and salty liquid water at the Phoenix landing site, Mars. *Journal of Geophysical Research: Planets*, *116*(E9), E09005. https://doi.org/10.1029/2011je003838

Stillman, D. E., & Grimm, R. E. (2011b). Radar penetrates only the youngest geological units on Mars. *Journal of Geophysical Research: Planets*, *116*(E3), E03001. https://doi.org/10.1029/2010je003661

Stillman, D. E., Grimm, R. E., & Dec, S. F. (2010). Low-frequency electrical properties of ice – Silicate mixtures. *Journal of Physical Chemistry*, *B114*(18), 6065–6073. https://doi.org/10.1021/jp9070778

Stillman, D. E., MacGregor, J. A., & Grimm, R. E. (2013a). Electrical response of ammonium-rich water ice. *Annals of Glaciology*, *54*(64), 21–26. https://doi.org/10.3189/2013aog64a204

Stillman, D. E., MacGregor, J. A., & Grimm, R. E. (2013b). The role of acids in electrical conduction through ice. *Journal of Geophysical Research: Earth Space*, *118*, 1–16. https://doi.org/10.1029/2012JF002603

Toner, J. D., Catling, D. C., & Light, B. (2014). The formation of supercooled brines, viscous liquids, and low-temperature perchlorate glasses in aqueous solutions relevant to Mars. *Icarus*, *233*, 36–47. https://doi.org/10.1016/j.icarus.2014.01.018

Wieczorek, M. A. (2008). Constraints on the composition of the martian south polar cap from gravity and topography. *Icarus*, *196*, 506–517.

Williams, K. K., & Greeley, R. (2004). Measurements of dielectric loss factors due to a Martian dust analog. *Journal of Geophysical Research*, *109*(E10), E10006. https://doi.org/10.1029/2002JE001957